Hybrid polarization induced transverse energy flow

Lyu, Yudong; Man, Zhongsheng; Zhao, Rui; Meng, Peiwen; Zhang, Wenfei; Ge, Xiaolu; Fu, Shenggui

DOI
10.1016/j.optcom.2020.126704

Publication date
2020

Document Version
Final published version

Published in
Optics Communications

Optics Communications 485 (2021) 126704

Contents lists available at ScienceDirect

Optics Communications

journal homepage: www.elsevier.com/locate/optcom

Hybrid polarization induced transverse energy flow

Yudong Lyu [a], Zhongsheng Man [a,c,*], Rui Zhao [a], Peiwen Meng [b], Wenfei Zhang [a], Xiaolu Ge [a], Shenggui Fu [a]

[a] School of Physics and Optoelectronic Engineering, Shandong University of Technology, Zibo 255000, China
[b] Optics Research Group, Delft University of Technology, Department of Imaging Physics, Lorentzweg 1, 2628CJ Delft, The Netherlands
[c] Collaborative Innovation Center of Light Manipulations and Application, Shandong Normal University, Jinan 250358, China

ARTICLE INFO

Keywords:
Diffractive optics
Polarization
Optical vortices
Optical tweezers or optical manipulation

ABSTRACT

Nonzero transverse energy flow, which describes phenomenon in which the energy flux of localized light propagates in a plane perpendicular to the optical axis, has attracted enormous interest recently due to its useful application in micromanipulation. We show that the appearance of transverse energy flow in the focal plane of an aplanatic high numerical aperture focusing system is possible. We demonstrate our approach by specially tailoring the input state of polarization. Calculations reveal that number of transverse energy flow rings is controllable and depend on azimuthal index of the input field, thereby giving rise to tunable manipulating locations in optical trapping.

1. Introduction

The energy flow of the optical field is always interesting and important, since it can be widely used in optical tweezers. In 1959, Richards and Wolf found that a linearly polarized plane wave can produce a region of negative propagation of light when focusing in an aplanatic high numerical aperture (NA) objective system, where a small negative magnitude for the longitudinal projection of the Poynting vector appears [1]. For the superposition of two Bessel beams with transverse electric (TE) and transverse magnetic (TM) polarizations, the expression for the Poynting vector indicates that under special conditions, light beam can propagate in the opposite direction of the optical axis [2]. For a tightly focused circularly polarized Laguerre-Gaussian beam, it has been demonstrated that negative values of the longitudinal component of the Poynting vector can be found near the focus [3]. Using the Richards–Wolf formulas for an arbitrary circularly polarized optical vortex with an integer topological charge m, Kotlyar et al. built explicit expressions for all components of the electric and magnetic field strength vectors near the focus, as well as expressions for the energy density and for the components of the Poynting vector in the focal plane. When $m = 2$, they found that the energy flux near the optical axis propagates in the reversed direction, rotating along a spiral around the optical axis [4]. Vector properties of light are also considered in the formation of a negative energy flux, such as cylindrical vector beams [5,6], which have locally linear states of polarization and exhibit perfect circular symmetry in the beam cross section [7,8].

In addition, there is current substantial interest in the transverse energy flow that is, generating customized energy flux that suit specific needs in practical applications [9–21]. As is known, the transverse energy flows in the focal plane of the tightly focused linearly and cylindrically polarized plane waves are always zero [9,11–13,17], hence the additional amplitude modulations should be introduced to generate and redistribute the transverse Poynting vector [9]. In addition, the vortex phase is also considered to manipulate the transverse components of the Poynting vector [10,20,21]. A recent development in the field explored the relation between transverse backflow and superoscillation [18]. Superoscillation is the phenomenon in which a band-limited signal locally oscillates faster than its fastest Fourier component. Based on a spectrally shifted suboscillatory function, Eliezer et al. constructed a light beam made of the superposition of modes having negative transverse momentum relative to a chosen axis of propagation and observed transverse optical backflow [18].

In this work, we theoretically explore the hybrid polarization induced transverse energy flow in the focal plane of a high NA focusing system. We introduce a family of vector optical fields with local state of polarization (SoP) exhibiting azimuthally-variant ellipticity. With the help of vectorical diffraction method, we present the electric and magnetic fields distributions of these beams focused by an aplanatic high NA objective lens then analyze the transverse energy flow of the focused field. It is shown that dark flower-like patterns on the axis for both electric and magnetic fields can be obtained. Furthermore, transverse energy flow appears in the focal plane, which is much different from that of the optical fields with locally linear SoP such as linearly and cylindrically polarized beams.

* Corresponding author at: School of Physics and Optoelectronic Engineering, Shandong University of Technology, Zibo 255000, China.
E-mail addresses: zsman@sdut.edu.cn (Z. Man), fushenggui@sdut.edu.cn (S. Fu).

https://doi.org/10.1016/j.optcom.2020.126704
Received 20 September 2020; Received in revised form 26 November 2020; Accepted 14 December 2020
Available online 17 December 2020

2. Light beams with hybrid SoP and corresponding tight-focusing analytical model

Polarization, as an intrinsic nature of light, plays an important role in the interaction of light with matter. Poincaré sphere (PS) shown in Fig. 1(a) is a simple and convenient geometric representation to describe all possible fundamental SoPs of a light beam, where s_1, s_2 and s_3 are the Stokes parameters of a point on PS in Cartesian coordinate system while 2Θ and 2Φ denote, respectively, the latitude and longitude angles of the point in spherical coordinate system. The poles of the PS represent the optical spin angular momentum eigenstates, i.e., the circular polarization. The equator denotes linear polarization, and any intermediate point between the poles and equator is elliptical polarization [22].

Apart from the homogeneous SoP, it is now known that light also support spatially-variant SoP, such as radially and azimuthally polarized beams. Theoretically, the SoP of any given polarized beam can be described using a linear combination of a pair of orthogonal base vectors with opposite phases. When referring to a light beam with hybrid SoP, it can be represented in terms of orthogonal linearly polarized unit vectors $\{\hat{\mathbf{e}}_1, \hat{\mathbf{e}}_2\}$ as [23–25]

$$\boldsymbol{E} = A\left[\exp(i\delta)\,\hat{\mathbf{e}}_1 + \exp(-i\delta)\,\hat{\mathbf{e}}_2\right], \tag{1}$$

where A is the relative amplitude distribution; δ represents the relative phase distributions of the unit vector that determines the polarization distributions of the light $\mathbf{E}$; the unit vectors $\hat{\mathbf{e}}_1$ and $\hat{\mathbf{e}}_2$ can be written as

$$\hat{\mathbf{e}}_1 = \cos\Phi\hat{\mathbf{e}}_x + \sin\Phi\hat{\mathbf{e}}_y, \tag{2}$$

$$\hat{\mathbf{e}}_2 = -\sin\Phi\hat{\mathbf{e}}_x + \cos\Phi\hat{\mathbf{e}}_y, \tag{3}$$

where $\hat{\mathbf{e}}_x$ and $\hat{\mathbf{e}}_y$ are the unit vectors along x and y axis, respectively. Eqs. (2) and (3) represent a pair of orthogonal base vectors since $\langle\hat{\mathbf{e}}_1|\hat{\mathbf{e}}_2\rangle = 0$, and the value of Φ determines the pair of orthogonal linear polarizations that act as the base vectors. Eq. (1) describes a linear combination of orthogonal linearly polarized optical vortexes of opposite topological charge. Factually, the function δ in Eq. (1) can have all kinds of distributions in theory. Here, the most fundamental case of $\delta = a\varphi + c$ is specially studied throughout this work, where a is the azimuthal index of the variable φ and c is a constant. As examples, Figs. 1(b)–1(c) depict three kinds of hybridly polarized (HP) beams with $(a, c) = (1, 0)$, $(1, \pi/2)$, and $(5, 0)$ when $\Phi = -\pi/4$, respectively. Apparently, all these beams exhibit quite different polarization distributions when compared with homogeneously polarized beams. First, any given point has a different SoP when located in different azimuthal directions. Second, linear, circular, and elliptical SoPs are mixed in the beam cross section.

Tight focusing is highly desirable, ranging from optical manipulation to imaging, as well as optical storage, and so on. When the input field is described by Eq. (1), the electromagnetic field at any point $P(r_P, \phi_P, z_P)$ near focus of an aplanatic high NA system can be expressed as [1,26]

$$\begin{bmatrix}\boldsymbol{E}_P\\ \boldsymbol{H}_P\end{bmatrix} = -\frac{ikf}{2\pi}\int_0^{\alpha}\int_0^{2\pi}\sqrt{\cos\theta}\,l_0(\theta)K(\varphi,\theta)\begin{bmatrix}\mathbf{V}_E\\ \mathbf{V}_H\end{bmatrix}\sin\theta\,d\varphi\,d\theta, \tag{4}$$

where k is the wavenumber and equals to $2\pi/\lambda$, λ being the wavelength in the image space; α represents the semi-aperture angle and equals to $\arcsin(\mathrm{NA}/n)$, NA being the numerical aperture of the objective lens and n the refractive index in the image space; φ and θ are, respectively, azimuthal angle with respect to x axis in the objective space and polar angle with respect to z axis; the function $l_0(\theta)$, which denotes the incident distribution, is considered as

$$l_0(\theta) = \exp\left[-\beta^2\left(\frac{\sin\theta}{\sin\alpha}\right)^2\right]J_1\left(2\beta\frac{\sin\theta}{\sin\alpha}\right). \tag{5}$$

Here, β is the ratio of the pupil radius to the beam waist, J_1 is the first order Bessel function of the first kind, and $K(\varphi, \theta)$ is the propagation factor in the image space given by

$$K(\varphi,\theta) = \exp\left\{ik\left[-r_P\sin\theta\cos(\varphi-\phi_P) + z_P\cos\theta\right]\right\}. \tag{6}$$

In Eq. (2), $\mathbf{V}_E$ and $\mathbf{V}_H$ represent, respectively, the electric and magnetic polarization vector in the tightly focused field, which derive from the contribution of polarization of the input beam. When the incident SoP is described by Eq. (1), the corresponding focusing electromagnetic polarization vectors are

$$\mathbf{V}_E = \begin{bmatrix}V_E^x\\ V_E^y\\ V_E^z\end{bmatrix}, \tag{7}$$

$$\begin{aligned}V_E^x &= [\cos(\Phi-\varphi)\cos\theta\cos\varphi - \sin(\Phi-\varphi)\sin\varphi]\exp[i(a\varphi+c)]\\ &\quad -[\sin(\Phi-\varphi)\cos\theta\cos\varphi + \cos(\Phi-\varphi)\sin\varphi]\exp[-i(a\varphi+c)]\end{aligned}, \tag{8}$$

$$\begin{aligned}V_E^y &= [\cos(\Phi-\varphi)\cos\theta\sin\varphi + \sin(\Phi-\varphi)\cos\varphi]\exp[i(a\varphi+c)]\\ &\quad -[\sin(\Phi-\varphi)\cos\theta\sin\varphi - \cos(\Phi-\varphi)\cos\varphi]\exp[-i(a\varphi+c)]\end{aligned}, \tag{9}$$

$$\begin{aligned}V_E^z &= [\cos(\Phi-\varphi)\sin\theta]\exp[i(a\varphi+c)]\\ &\quad -[\sin(\Phi-\varphi)\sin\theta]\exp[-i(a\varphi+c)]\end{aligned}, \tag{10}$$

$$\mathbf{V}_H = \sqrt{\frac{\varepsilon}{\mu}}\begin{bmatrix}V_H^x\\ V_H^y\\ V_H^z\end{bmatrix}, \tag{11}$$

$$\begin{aligned}V_H^x &= [-\sin(\Phi-\varphi)\cos\theta\cos\varphi - \cos(\Phi-\varphi)\sin\varphi]\exp[i(a\varphi+c)]\\ &\quad -[\cos(\Phi-\varphi)\cos\theta\cos\varphi - \sin(\Phi-\varphi)\sin\varphi]\exp[-i(a\varphi+c)]\end{aligned}, \tag{12}$$

$$\begin{aligned}V_H^y &= [-\sin(\Phi-\varphi)\cos\theta\sin\varphi + \cos(\Phi-\varphi)\cos\varphi]\exp[i(a\varphi+c)]\\ &\quad -[\cos(\Phi-\varphi)\cos\theta\sin\varphi + \sin(\Phi-\varphi)\cos\varphi]\exp[-i(a\varphi+c)]\end{aligned}, \tag{13}$$

$$\begin{aligned}V_H^z &= [-\sin(\Phi-\varphi)\sin\theta]\exp[i(a\varphi+c)]\\ &\quad -[\cos(\Phi-\varphi)\sin\theta]\exp[-i(a\varphi+c)]\end{aligned}, \tag{14}$$

where ε and μ are the electric permittivity and magnetic permeability, respectively.

3. Energy flow

In terms of the 3D electric and magnetic fields expressed by Eqs. (7)–(10) and (11)–(14), we now investigate the energy flow, which is obtained from a determination of the time-averaged Poynting vector [1, 27–29]

$$\boldsymbol{S} \propto \mathrm{Re}\left(\boldsymbol{E}_P \times \boldsymbol{H}_P^*\right), \tag{15}$$

where the asterisk represents complex conjugation. Now, we can calculate the energy flux using Eqs. (1)–(15). For our focusing system, we chose NA = 0.95, $n = 1$, $\lambda = 532$ nm, $f = 1.6$ mm, and $\beta = 1$ in the following calculations.

We first examine the focal distributions of the electromagnetic fields. Fig. 2 gives normalized electric field intensity distributions in the focal plane of two input HP beams with $(a, c) = (1, 0)$ and $(1, \pi/2)$, respectively. Strangely, both these HP beams can generate square-shaped patterns for the total fields, which are of course the vector sum of the x, y and longitudinal components. In the case $c = 0$, the longitudinal component primarily contributes to the on-axis field, which results in a flat-topped pattern for the total field. In the case $c = \pi/2$, however, the distribution has multiple foci, with an on-axis null intensity for the longitudinal component, which leads to an optical hollow distribution for the total field. Fig. 3 depicts the corresponding magnetic field intensity distributions in the focal plane for the aforementioned two input beams. Interestingly, the magnetic fields for $(a, c) = (1, 0)$ and

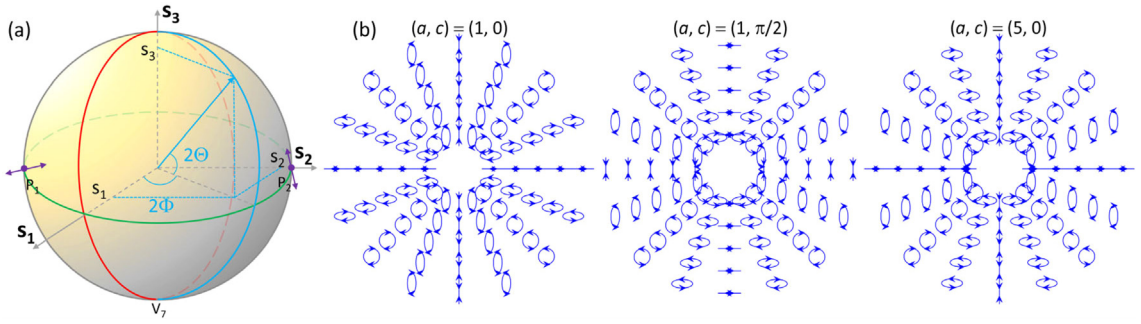

Fig. 1. (a) Poincaré sphere representation for plane waves with arbitrary fundamental SoPs. (b) Polarization distributions of three HP beams with (a, c) = (1, 0), (1, $\pi/2$), and (5, 0), respectively.

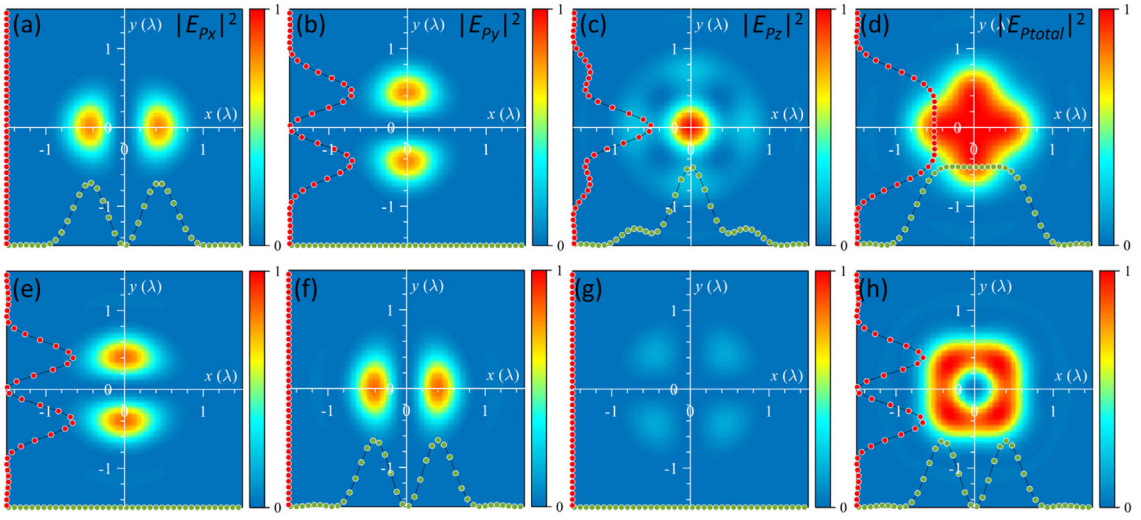

Fig. 2. Calculated electric field intensity distributions in the focal plane of tightly focused input fields with (a, c) = (1, 0) and (1, $\pi/2$) (upper and lower rows, respectively). From left to right, the four columns show the x, y, and z components and the total field. The insets for each image depict the normalized intensity profiles along the x (green curve) and the y axes (red curve), respectively. All intensity distributions are normalized to the maximum intensity in the focal plane for each input light mode.. (For interpretation of the references to color in this figure legend, the reader is referred to the web version of this article.)

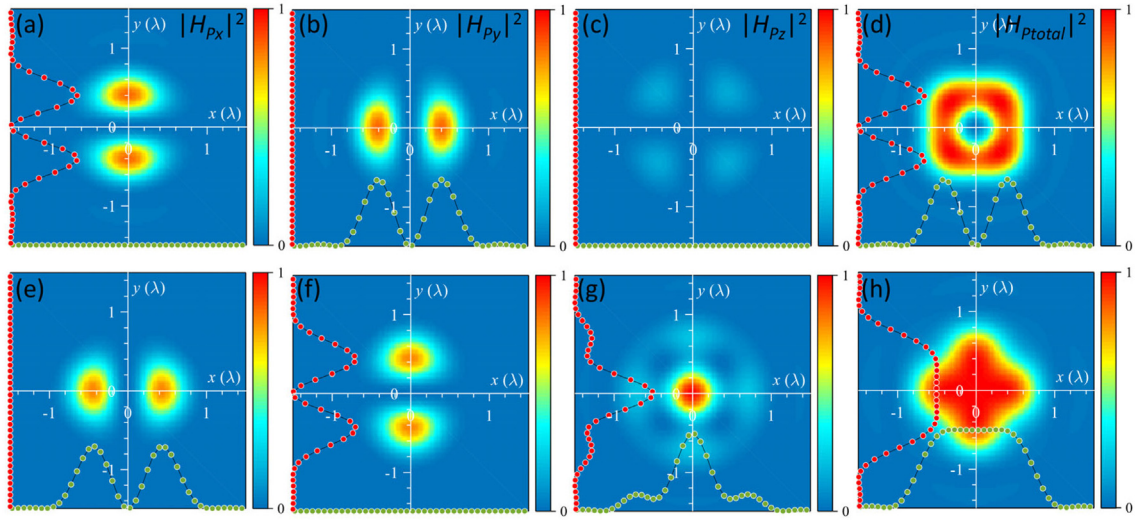

Fig. 3. Calculated magnetic fields intensity distributions in the focal plane of tightly focused input fields with (a, c) = (1, 0) and (1, $\pi/2$) (upper and lower rows, respectively). From left to right, the four columns show the x, y, and z components and the total field. The insets for each image depict the normalized intensity profiles along the x (green curve) and the y axes (red curve), respectively. All intensity distributions are normalized to the maximum intensity in the focal plane for each input light mode.. (For interpretation of the references to color in this figure legend, the reader is referred to the web version of this article.)

(1, $\pi/2$) are similar to the electric fields of input beam with (a, c) = (1, $\pi/2$) and (1, 0), respectively.

Now we discuss the energy flow of the HP beams, in particular the transverse energy flow, which is useful in manipulating the absorptive

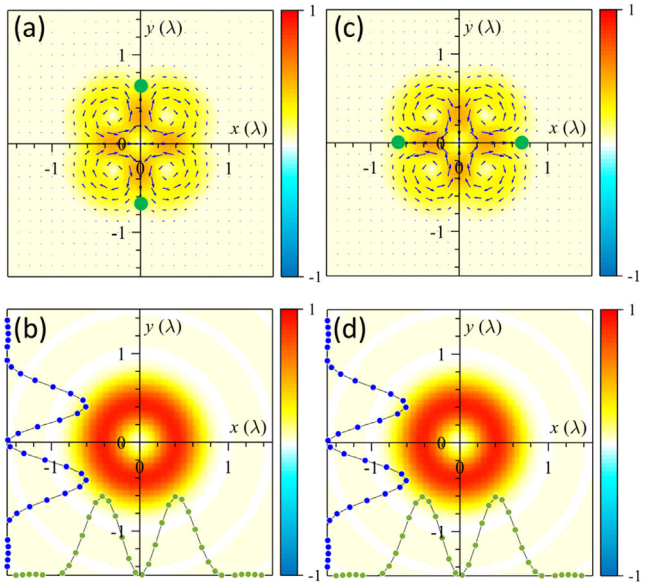

Fig. 4. Energy flow distributions of the tightly focused input optical fields with (a, c) = (1, 0) and (1, $\pi/2$) (left and right columns, respectively). The upper and lower rows depict, respectively, the transverse and longitudinal energy flows. The direction of the transverse energy flow is indicated by black arrows. The insets for the longitudinal energy flow distributions depict the profiles along the x (green curve) and the y axes (red curve), respectively. All energy flow distributions are normalized by the maximum energy flow in the focal plane for each input light mode.. (For interpretation of the references to color in this figure legend, the reader is referred to the web version of this article.)

particle in optical tweezers. By calculations, we find that the transverse energy flow always exists for the proposed HP beams, in contrast to incident fields with locally linear SoP. The Poynting vectors of the tightly focused fields in the focal plane when (a, c) = (1, $\pi/2$) and (1, 0) are shown in Fig. 4. We can see in Figs. 4(a) and 4(c) that when a = 1, there are four transverse energy flow rings arising from spin–orbit conversion [30,31], two of them are clockwise while the other two are anticlockwise. Finally, the energy flows to two fixed locations marked by green points, implying the absorptive particles can be transported to different locations along different routes. In addition, the polarization handedness changes 4 times per round when a = 1 shown in Fig. 1. And in Fig. 4, four respective singularity points are depicted, around which the transverse energy flow rotates in different directions. We can see from Figs. 4(b) and 4(d) that this method does not allow obtaining a negative longitudinal component of the Poynting vector [32].

The above investigations focus on the cases when the azimuthal index of the HP beams equals to 1, and two fixed manipulating locations can be obtained. The SoP of the HP beams with a higher-order azimuthal index of variable φ becomes more complicated. Fig. 5 shows the calculated focal distributions of the total electric and magnetic fields of tightly focused input fields with a = 2, 3, 4, and 5 when c = 0. Obviously, they are non-uniform hollow intensity distributions with dark flower-like patterns for both the electric and magnetic fields for all the four higher-order HP incident beams. The corresponding transverse and longitudinal components of the Poynting vectors for the above four input fields are depicted in Fig. 6. It can be seen from the transverse energy flow that the number of energy flow rings increases with the increase of the azimuthal index a, which can be used to trap and transport multiple absorptive particles in different routes. The number of transverse energy flow rings is equal to 4a, and the number of fixed manipulating locations (green points) is 2a, as shown in the upper row in Fig. 6. By contrary, the longitudinal energy flow always exhibits a single ring distribution, and the size of the longitudinal energy flow ring will gradually increase as a increases.

As a increases, the transverse component of the Poynting vector becomes stronger than the longitudinal component. This trend is shown in Fig. 7, which show the ratio of the maximums of the transverse and longitudinal components of the Poynting vector versus the azimuthal index a when c = 0.

In addition to the wide range of academic interest and huge potential applications, the experimental realization of the proposed approach is vital. In this method, the key is that the input field has a hybrid state of polarization. Fortunately, great success has been achieved in the creation of vector beams [33,34], in particular HP beams [23,35], which provides a strong guarantee for the generation of transverse energy flow.

4. Conclusions

To summarize, we demonstrated the appearance of the transverse energy flow within the tightly focused field of HP beams. The proposed

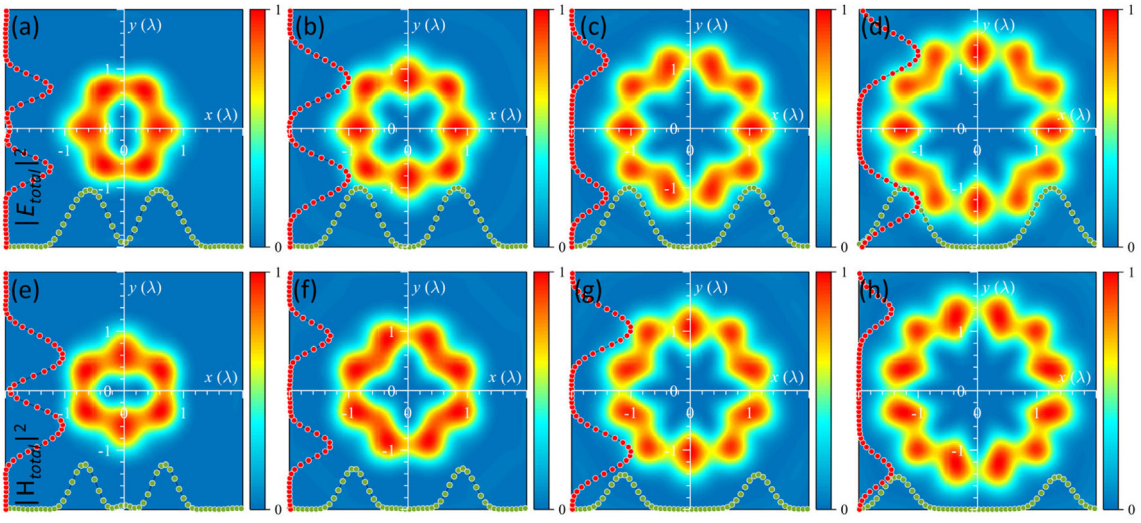

Fig. 5. Calculated electric and magnetic fields intensity distributions in the focal plane of the total of tightly focused input fields with (a, c) = (2, 0), (3, 0), (4, 0), and (5, 0) (from left to right column, respectively). The upper and lower rows depict, respectively, the total electric and magnetic fields. The insets for each image are the normalized intensity profiles along the x (green curve) and the y axes (red curve), respectively. All intensity distributions are normalized to the maximum intensity in the focal plane for each input light mode.. (For interpretation of the references to color in this figure legend, the reader is referred to the web version of this article.)

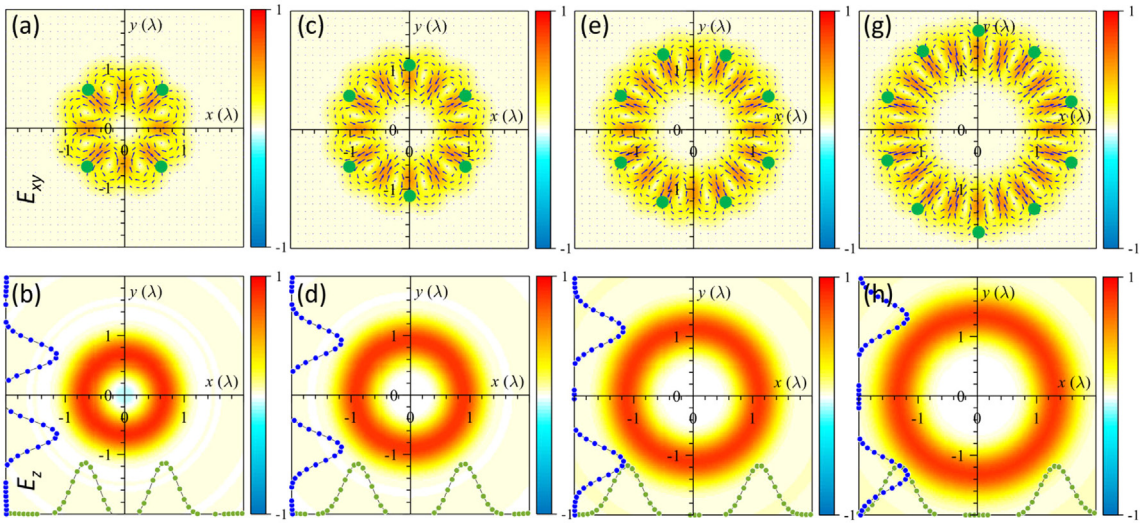

Fig. 6. Energy flow distributions of the tightly focused input optical fields with (a, c) = (2, 0), (3, 0), (4, 0), and (5, 0) (from left to right column, respectively). The upper and lower rows depict, respectively, the transverse and longitudinal energy flows. The direction of the transverse energy flow is indicated by black arrows. The insets for the longitudinal energy flow distributions depict the profiles along the x (green curve) and the y axes (red curve), respectively. All energy flow distributions are normalized by the maximum energy flow in the focal plane for each input light mode.. (For interpretation of the references to color in this figure legend, the reader is referred to the web version of this article.)

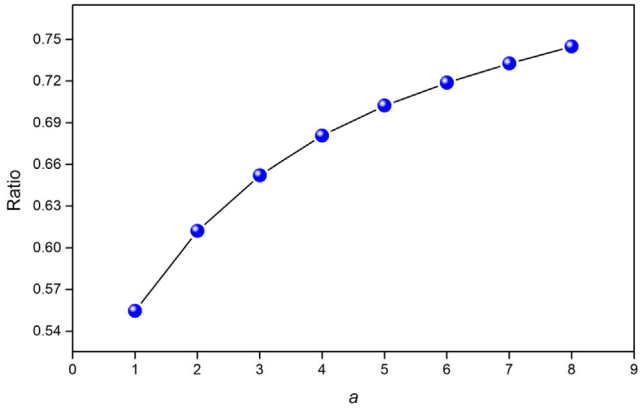

Fig. 7. Ratio of the maximums of the transverse and longitudinal components of the Poynting vector versus the azimuthal index a when $c = 0$.

method require that the input beam has a hybrid state of polarization, which is more complexed compared with other polarization beams, however, no other additional amplitude or phase modulations are needed. With the help of Richards–Wolf vectorial method, we presented an analytical model for the high NA focusing system to evaluate all three components of the electric and magnetic field strengths and Poynting vector in the focal region. By numerically calculating the energy density and energy flux in the focal plane of an aplanatic optical system based on our theoretical model, we demonstrated that dark flower-like patterns on the axis for both electric and magnetic fields can be obtained. Furthermore, there is obvious transverse energy flow for the input HP beams, which is much different from that of the optical field with locally linear SoP such as linearly and cylindrically polarized beams, where no transverse energy flow can be found. This work not only broadens the structured optical fields, but also has potential applications including optical fabrication and micromanipulation.

Declaration of competing interest

The authors declare that they have no known competing financial interests or personal relationships that could have appeared to influence the work reported in this paper.

Acknowledgments

This work was supported by the National Natural Science Foundation of China (NSFC) (12074224, 61975128, 62005146); and the Natural Science Foundation of Shandong Province, China (ZR2017MA051).

References

[1] B. Richards, E. Wolf, Electromagnetic diffraction in optical systems, II. Structure of the image field in an aplanatic system, Proc. R. Soc. Lond. Ser. A Math. Phys. Eng. Sci. 253 (1959) 358–379.
[2] A.V. Novitsky, D.V. Novitsky, Negative propagation of vector Bessel beams, J. Opt. Soc. Amer. A 24 (2007) 2844–2849.
[3] P.B. Monteiro, P.A. Maia Neto, H.M. Nussenzveig, Angular momentum of focused beams: Beyond the paraxial approximation, Phys. Rev. A 79 (2009) 033830.
[4] V.V. Kotlyar, A.A. Kovalev, A.G. Nalimov, Energy density and energy flux in the focus of an optical vortex: reverse flux of light energy, Opt. Lett. 43 (2018) 2921–2924.
[5] S.N. Khonina, A.V. Ustinov, S.A. Degtyarev, Inverse energy flux of focused radially polarized optical beams, Phys. Rev. A 98 (2018) 043823.
[6] V.V. Kotlyar, S.S. Stafeev, A.G. Nalimov, Energy backflow in the focus of a light beam with phase or polarization singularity, Phys. Rev. A 99 (2019) 033840.
[7] Q. Zhan, Cylindrical vector beams: from mathematical concepts to applications, Adv. Opt. Photon. 1 (2009) 1–57.
[8] Z. Man, S. Fu, G. Wei, Focus engineering based on analytical formulae for tightly focused polarized beams with arbitrary geometric configurations of linear polarization, J. Opt. Soc. Amer. A 34 (2017) 1384–1391.
[9] X. Jiao, S. Liu, Q. Wang, X. Gan, P. Li, J. Zhao, Redistributing energy flow and polarization of a focused azimuthally polarized beam with rotationally symmetric sector-shaped obstacles, Opt. Lett. 37 (2012) 1041–1043.
[10] X. Gao, Y. Pan, G. Zhang, M. Zhao, Z. Ren, C. Tu, Y. Li, H. Wang, Redistributing the energy flow of tightly focused ellipticity-variant vector optical fields, Photon. Res. 5 (2017) 640–648.
[11] Z. Man, Z. Bai, S. Zhang, X. Li, J. Li, X. Ge, Y. Zhang, S. Fu, Redistributing the energy flow of a tightly focused radially polarized optical field by designing phase masks, Opt. Express 26 (2018) 23935–23944.
[12] W. Yuan, Z. Man, Manipulating the magnetic energy density and energy flux by cylindrically symmetric state of polarization, Optik 185 (2019) 208–214.
[13] Z. Man, X. Li, S. Zhang, Z. Bai, Y. Lyu, J. Li, X. Ge, Y. Sun, S. Fu, Manipulation of the transverse energy flow of azimuthally polarized beam in tight focusing system, Opt. Commun. 431 (2019) 174–180.
[14] Z. Man, X. Dou, S. Fu, Pancharatnam-Berry phase shaping for control of the transverse enhancement of focusing, Opt. Lett. 44 (2019) 427–430.
[15] Y. Pan, X. Gao, G. Zhang, Y. Li, C. Tu, H. Wang, Spin angular momentum density and transverse energy flow of tightly focused kaleidoscope-structured vector optical fields, APL Photon. 4 (2019) 096102.
[16] Z. Man, P. Meng, S. Fu, Creation of complex nano-interferometric field structures, Opt. Lett. 45 (2020) 37–40.

[17] Z. Man, X. Dou, H.P. Urbach, The evolutions of spin density and energy flux of strongly focused standard full Poincaré beams, Opt. Commun. 458 (2020) 124790.
[18] Y. Eliezer, T. Zacharias, A. Bahabad, Observation of optical backflow, Optica 7 (2020) 72–76.
[19] Z. Man, Z. Xi, X. Yuan, R.E. Burge, H.P. Urbach, Dual coaxial longitudinal polarization vortex structures, Phys. Rev. Lett. 124 (2020) 103901.
[20] A.V. Ustinov, V.G. Niziev, S.N. Khonina, S.V. Karpeev, Local characteristics of paraxial Laguerre-Gaussian vortex beams with zero total angular momentum, J. Mod. Opt. 66 (2019) 1961–1972.
[21] S.N. Khonina, A.V. Ustinov, S.G. Volotovskiy, N.A. Ivliev, V.V. Podlipnov, Influence of optical forces induced by paraxial vortex Gaussian beams on the formation of a microrelief on carbazole-containing azopolymer films, Appl. Opt. 59 (2020) 9185–9194.
[22] M. Born, E. Wolf, Principles of Optics, seventh ed., Cambridge University, 1999.
[23] X. Wang, Y. Li, J. Chen, C. Guo, J. Ding, H. Wang, A new type of vector fields with hybrid states of polarization, Opt. Express 18 (2010) 10786–10795.
[24] G. Milione, H.I. Sztul, D.A. Nolan, R.R. Alfano, Higher-order Poincaré sphere, Stokes parameters, and the angular momentum of light, Phys. Rev. Lett. 107 (2011) 053601.
[25] Z. Man, Z. Bai, J. Li, S. Zhang, X. Li, X. Ge, S. Fu, Focus shaping by tailoring arbitrary hybrid polarization states that have a combination of orthogonal linear polarization bases, Appl. Opt. 57 (2018) 3047–3055.
[26] Z. Man, C. Min, L. Du, Y. Zhang, S. Zhu, X. Yuan, Sub-wavelength sized transversely polarized optical needle with exceptionally suppressed side-lobes, Opt. Express 24 (2016) 874–882.
[27] V.V. Kotlyar, S.S. Stafeev, A.G. Nalimov, A.A. Kovalev, A.P. Porfirev, Mechanism of formation of an inverse energy flow in a sharp focus, Phys. Rev. A 101 (2020) 033811.
[28] M.V. Berry, Optical currents, J. Opt. A: Pure Appl. Opt. 11 (2009) 094001.
[29] O.V. Angeisky, A.Y. Bekshaev, P.P. Maksimyak, A.P. Maksimyak, S.G. Hanson, C.Y. Zenkova, Orbital rotation without orbital angular momentum: mechanical action of the spin part of the internal energy flow in light beams, Opt. Express 20 (2012) 3563–3571.
[30] T.A. Nieminen, A.B. Stilgoe, N.R. Heckenberg, H. Rubinsztein-Dunlop, Augular momentum of a strongly focused Gaussian beam, J. Opt. A: Pure Appl. Opt. 10 (2008) 115005.
[31] V.V. Kotlyar, A.G. Nalimov, S.S. Stafeev, Exploiting the circular polarization of light to obtain a spiral energy flow at the subwavelength focus, J. Opt. Soc. Amer. B 36 (2019) 2850.
[32] S.N. Khonina, A.V. Ustinov, Increased reverse energy flux area when focusing a linearly polarized annular beam with binary plates, Opt. Lett. 44 (2019) 2008.
[33] X. Wang, J. Ding, W. Ni, C. Guo, H. Wang, Generation of arbitrary vector beams with a spatial light modulator and a common path interferometric arrangement, Opt. Lett. 32 (2007) 3549–3551.
[34] U. Levy, C. Tsai, L. Pang, Y. Fainman, Engineering space-variant inhomogeneous media for polarization control, Opt. Lett. 29 (2004) 1718–1720.
[35] S.N. Khonina, A.V. Ustinov, S.A. Fomchenkov, A.P. Porfirev, Formation of hybrid higher-order cylindrical vector beams using binary multi-sector phase plates, Sci. Rep. 8 (2018) 14320.